PHYSICAL REVIEW B **68**, 020103(R) (2003)

Pressure-induced phase transitions and templating effect in three-dimensional organic-inorganic hybrid perovskites

Yongjae Lee,[1] David B. Mitzi,[2] Paris W. Barnes,[3] and Thomas Vogt[1]
[1]*Physics Department, Brookhaven National Laboratory, Upton, New York 11973-5000, USA*
[2]*IBM T. J. Watson Research Center, P.O. Box 218, Yorktown Heights, New York 10598, USA*
[3]*Department of Chemistry, The Ohio State University, Columbus, Ohio 43210, USA*

(Received 7 March 2003; published 29 July 2003)

Pressure-induced structural changes of conducting halide perovskites $(CH_3NH_3)SnI_3$, $(CH_3NH_3)_{0.5}(NH_2CH{=}NH_2)_{0.5}SnI_3$, and $(NH_2CH{=}NH_2)SnI_3$, have been investigated using synchrotron x-ray powder diffraction. In contrast to low-temperature structural changes, no evidence of an increased ordering of the organic cations was observed under pressure. Instead, increase in pressure results first in a ReO_3-type doubling of the primitive cubic unit cell, followed by a symmetry distortion, and a subsequent amorphization above 4 GPa. This process is reversible and points towards a pressure-induced templating role of the organic cation. Bulk compressions are continuous *across* the phase boundaries. The compressibilities identify these hybrids as the most compressible perovskite system ever reported. However, the Sn-I bond compressibility in $(CH_3NH_3)SnI_3$ shows a discontinuity *within* the supercell phase. This is possibly due to an electronic localization.

DOI: 10.1103/PhysRevB.68.020103 PACS number(s): 61.50.Ks, 62.50.+p, 51.35.+a, 81.07.Pr

INTRODUCTION

Hybrid perovskites are nanoscale composites of inorganic and organic components in which the effective dimensionality of the inorganic framework can be controlled from zero to three dimensions, resulting in various magnetic, luminescent, and conducting properties.[1,2] The ordering and hydrogen bonding of the organic cations are known to change as a function of temperature, giving rise to various structural phase transitions.[3–6] Knowledge of pressure-induced structural and electronic transitions of the organic-inorganic hybrids is, however, scarce.[7] We have initiated a systematic study to explore the high-pressure behaviors of various hybrid perovskites using monochromatic synchrotron x-ray powder diffraction. Conducting tin(II)-iodide-based 3D hybrid cubic perovskites $(M_xF_{1\text{-}x})SnI_3$ ($M = CH_3NH_3^+$, $F = NH_2CH{=}NH_2^+$), were chosen for the initial investigations.[8,9] These structures consist of corner-sharing SnI_6 octahedra and organic cations located at an A site within the cubooctahedral cages (Fig. 1). At room temperature, isotropic dynamic reorientations of the organic cations occur since the symmetry of the free organic cations does not match the O_h site symmetry of the A site in the cubic perovskite structure. Upon cooling, the structures distort and the motions of the organic cations become more restricted. Changes in the electrical resistivity with temperature were reported concomitant with the increased ordering of the organic cation.[8,10]

EXPERIMENTAL METHOD

Polycrystalline samples of $M SnI_3$, $M_{0.5}F_{0.5}SnI_3$, and $F SnI_3$ were prepared by a precipitation method using appropriate hydroiodic acid solution mixtures.[8,9] *In situ* high pressure synchrotron x-ray powder diffraction experiments were performed using a diamond anvil cell (DAC) at the X7A beamline of the National Synchrotron Light Source (NSLS) at Brookhaven National Laboratory (BNL). Details regarding the experimental setup are given elsewhere.[11] Since the samples are air sensitive and decompose in air within several hours, care was taken to minimize the exposure time during the sample loading, and a fully fluorinated polymer (3M Fluorinert™ FC-75) was used as a pressure transmission fluid. The pressure at the sample was measured by detecting the shift in the $R1$ emission line of the included ruby chips. The hydrostatic limit for Fluorinert is generally quoted to be around 1.5 GPa,[12,13] but others report its extended hydrostaticity with only minor broadening of diffraction peaks observed above 4.7 GPa.[14] In our experiments, no evidence of nonhydrostatic behavior or pressure anisotropy was detected, and the $R1$ peaks from three to four included ruby chips remained strong and sharp with deviations less than ± 0.1 GPa. The extended hydrostaticity of Fluorinert in our experiments may be related to the fact that these hybrid perovskites are softer than the glass that Fluorinert forms under pressure (see next section). Use of other nonoxidizing pressure fluids such as petroleum ether (hydrostatic up to 6 GPa) or pentane-isopentane mixture (hydrostatic up to 7.4 GPa) may well be considered in the future experiments. Structural models of the $M SnI_3$ sample were refined using the Rietveld method[15] and the unit cell parameters of the F-containing compounds were determined by whole pattern fitting using the LeBail method.[16] Bulk moduli and pressure derivatives were calculated by fitting the normalized volumes to a third-order Birch-Murnaghan equation of state,[17] and no constraints or weights were used in the fit.

RESULTS AND DISCUSSION

The pressure-dependent changes of the $M SnI_3$ powder diffraction patterns are shown in Fig. 1, and the changes of its unit cell lengths are depicted in Fig. 2 [see Supplemental Fig. 1 (Ref. 32) for $M_{0.5}F_{0.5}SnI_3$ and $F SnI_3$ compounds]. In all cases, the ambient pressure primitive cubic unit cell transforms to a body-centered cubic one, with supercell reflections appearing after 0.5 GPa. Further increase in pressure

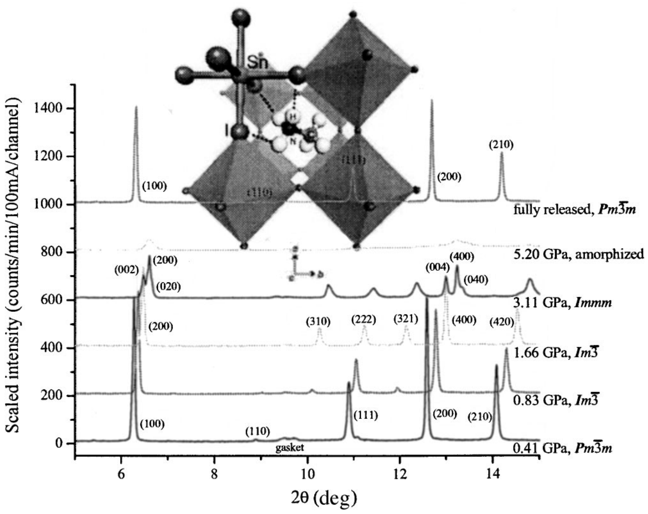

FIG. 1. Details of the changes in the synchrotron x-ray powder diffraction patterns of $(CH_3NH_3)SnI_3$ as a function of pressure (right). The inset shows perspective view of the unit cell of $(CH_3NH_3)SnI_3$.

results in an orthorhombic distortion of MSnI$_3$ after 2.2 GPa (Fig. 1). No mixed phase regions before or after the phase transitions were detected. In the case of FSnI$_3$, the lowering from cubic to tetragonal symmetry begins near 1.9 GPa. The pressure evolution of the mixed cation sample $M_{0.5}F_{0.5}$SnI$_3$, is somewhat different from those observed for the two end members. The tetragonal distortion occurs as early as 0.8 GPa and increases as the pressure increases up to 4.0 GPa. In all cases, anisotropic peak broadening is observed upon pressure increase, and above 4.0 GPa, apparently under sustained hydrostatic conditions based on the sharp ruby peaks, all three samples become x-ray amorphous; only weak intensities of the original $h00$ reflections remain and a newly formed broad background originating from the diffuse scattering appears (Fig. 1). The phase transition and amorphization sequence is reversible. The pressure-volume data do not show any apparent discontinuities, suggesting the pressure-induced phase transitions are second or higher order [Fig. 2 and Supplemental Fig. 1 (Ref. 32)]. When the bulk moduli and pressure derivatives are calculated over the entire pressure range observed up to the amorphization, the resulting fit to the normalized volume is within $\sigma(V/V_0)$ at each pressure point, implying no mechanical discontinuity. The derived overall bulk moduli K_0^{overall} are 12.6(7), 8.0(7), and 11.5(7) GPa for MSnI$_3$, FSnI$_3$, and $M_{0.5}F_{0.5}$SnI$_3$ samples, respectively. This demonstrates the highly compressible nature of these hybrid halide compounds. In particular, FSnI$_3$ is three times more compressible than NaCl ($K_0 = 23.5$ GPa)[18] and has the smallest bulk modulus observed in any reported perovskite-related structure. This is partly related to the decreased framework stability upon substitution of the larger formamidinium cation in the A site. During the volume contraction under pressure, no indications of an increased order in the isotropic dynamic reorientations of the organic cations were detected. Instead, the organic cations simply act as templates for the SnI$_6$ octahedral frameworks under pressure. Similar effects have been observed in several clathrasils and zeolites, where guest molecules or simple cations within pores are identified as rigid organizing centers for reversible pressure-induced amorphization processes.[19–21] Since the pressure-induced structural evolutions of these halide perovskites are distinct from the temperature-driven changes, variations of resistivity and other properties as a function of pressure are also expected to be different.

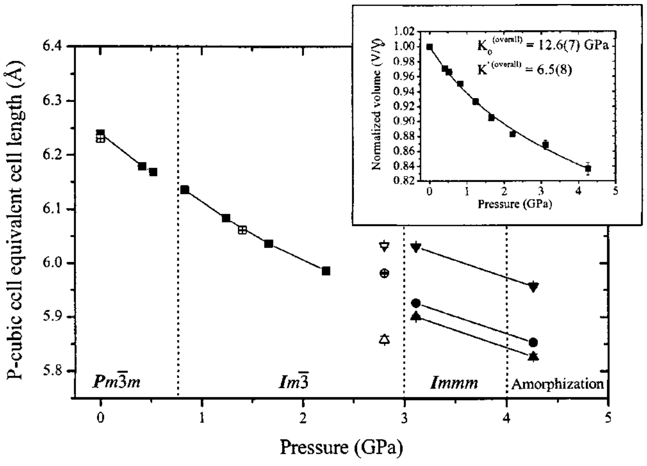

FIG. 2. Pressure dependence of the P-cubic equivalent unit cell edge lengths of MSnI$_3$. Closed (open) symbols represent pressure increase (release). The inset shows a fit of bulk modulus and pressure derivative on V/V_0. ESD's are multiplied by 3 at each value.

Systematic absences and group-subgroup relationships suggest the following pressure-induced phase transition sequences: $Pm\overline{3}m$–$Im\overline{3}$–$Immm$ for MSnI$_3$, $Pm\overline{3}m$–$Im\overline{3}$–$I4/mmm$ for FSnI$_3$ and $M_{0.5}F_{0.5}$SnI$_3$. In agreement with Aleksandrov's as well as Howard and Stokes' classifications,[22,23] the lower pressure phase transitions from primitive to body-centered cubic are observed as continuous second-order phase transitions. The driving force for this transition is probably related to the relief of strain in the Sn-I bond by displacing the iodine off the ⟨100⟩ axis, rather than to a different ordering of the organic cations in the symmetrically inequivalent A sites in the supercell phase. In fact, the same $Pm\overline{3}m$ to $Im\overline{3}$ transition under pressure is observed in ReO$_3$, a perovskite framework without occupied A site.[24] This demonstrates the "soft" nature of the organic cations under pressure. The second pressure-induced phase transition, involving the symmetry reduction to orthorhombic $Immm$ or tetragonal $I4/mmm$, however, has not been predicted to occur at all. We argue that it is a consequence of the interplay between the tilting and distortion of the SnI$_6$ octahedra as well as the increased templating effect of the organic cation, with the latter driving the reversible amorphization at higher pressures.

Rietveld refinements were performed using *in situ* high pressure x-ray diffraction data on a MSnI$_3$ sample (Table I, Fig. 3). The disordered M cations of the A site were modeled using spherical pseudoatoms with similar scattering factors on the ideal positions. In contrast to the continuous variation of the unit cell lengths and volume (Fig. 2), Sn-I distances clearly show two distinct regions with different compress-

TABLE I. Rietveld refinement results of $M\mathrm{SnI}_3$ as a function of pressure. ESD's are in parentheses. Fractional coordinates for iodine atoms. Sn atoms are at 0,0,0 in $Pm\overline{3}m$ phase and at 0.25,0.25,0.25 in $Im\overline{3}$ phase. M cations are modeled using Al atom at $m\overline{3}m$, and at $m\overline{3}$ and mmm sites in $Pm\overline{3}m$, and $Im\overline{3}$ phases, respectively. ${}_{\mathrm{w}}R_p$ (R_p) and χ^2 are in the range of 5.6–8.4% (4.2–5.8%) and 6.8–24.7, respectively. Analyses on $F\mathrm{SnI}_3$ and $M_{0.5}F_{0.5}\mathrm{SnI}_3$ are underway.

Pressure (GPa)	space group	Cell length (Å)	x,y,z
0.41	$Pm\overline{3}m$	$a=6.17911(6)$	0,0,1/2
0.52	$Pm\overline{3}m$	$a=6.16896(6)$	0,0,1/2
0.83	$Im\overline{3}$	$a=12.2716(1)$	0,0.2380(6),0.2634(5)
1.24	$Im\overline{3}$	$a=12.1668(2)$	0,0.2194(5),0.2734(6)
1.66	$Im\overline{3}$	$a=12.0730(3)$	0,0.2124(4),0.2766(5)
2.23	$Im\overline{3}$	$a=11.9717(3)$	0,0.2072(4),0.2783(5)
3.11	$Immm$	$a=11.853(1)$ $b=11.803(1)$ $c=12.062(1)$	

ibilities [Fig. 3 and Supplemental Fig. 2 (Ref. 32)]. Intriguingly, this change in the Sn-I bond compression occurs *after* the supercell transition near 1.2 GPa and possibly involves a minute increase in the Sn-I distance (of 6σ) upon pressure increase from 0.8 to 1.2 GPa. On the other hand, the A-site-to-iodine distances shows continuous variations with sets of long-, intermediate- and short-distances from the $6b$ site (0,1/2,0) developing upon the supercell transition [Supplemental Fig. 2 (Ref. 32)]. O'Keeffe *et al.* has shown that the variation of octahedral tilt with pressure in orthorhombic perovskites depends on the strength of the two bond compressibilities $\beta_{A\text{-O}}$ and $\beta_{B\text{-O}}$.[25] If the A site is more compressible, $\beta_{A\text{-O}}>\beta_{B\text{-O}}$, the tilting should increase with pressure and the structure will distort away from cubic symmetry. If the bond compressibilities are reversed in magnitude, tilting should decrease with pressure. Bond compressibilities $\beta_0=-(\partial l/\partial P)/l_0$, for Sn-I and M-I were calculated by fitting the normalized Sn-I bond lengths and the idealized A-site-to-iodine distance of $M\mathrm{SnI}_3$ data to a linearlized second-order Birch-Murnaghan equation of state using the pressure derivative determined from pressure-volume data.[26] We find that the relationship between bond compressibilities and octahedral tilting is indeed observed in $M\mathrm{SnI}_3$; in the cubic aristotype region, the compressibilities of the Sn-I and M-I bonds are the same within one sigma, and the subsequent decrease in the Sn-I compressibility and resulting $\beta_{A\text{-O}}>\beta_{B\text{-O}}$ relationship is accompanied by a departure of Sn-I-Sn angle away from the aristotype 180° (Fig. 3). This results in an increase of the SnI_6 octahedral tilt that develops in-phase along the respective axes.[27,28] However, the onset of octahedral tilting, which corresponds to the supercell transition near 0.8 GPa, was excluded in calculating the Sn-I bond compressibility in the cubic supercell region due to the reason outlined above (Fig. 3). The deviation from cubic symmetry and the accompanying changes in the tilt system in the higher pressure orthorhombic phase indicates changes in the $\beta_{A\text{-O}}>\beta_{B\text{-O}}$ relationship. However, we were not able to extract any reliable atomistic structural information of the orthorhombic phase due to the increased anisotropic broadening. The use of pair-distribution functions will be potentially important in probing such local structural rearrangements.

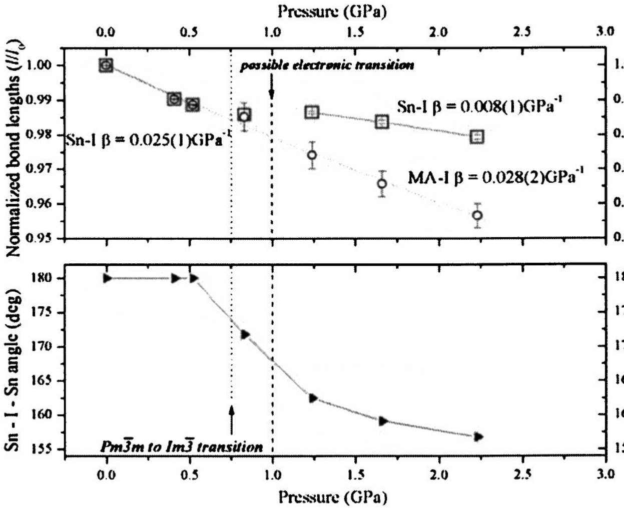

FIG. 3. Pressure dependence of the average Sn-I and A-site-to-iodine distances normalized to ambient pressure values (upper) and the variation of Sn-I-Sn angle (lower). ESD's are multiplied by 3 at each value.

As mentioned above, $\beta_{\text{Sn-I}}$ shows two distinct compression behaviors, and the bond compressibility below 0.8 GPa is about three times larger than the one above that pressure (Fig. 3). The increase in the Sn-I bond length within the supercell region between 0.8 and 1.2 GPa and the subsequent reduction in the bond compressibility may indicate a change in the electronic structure of the Sn atom. This is in line with the recent observation of a phase transition sequence in $\mathrm{Fe_2O_3}$ hematite where the isostructural electronic transition (possibly HS to LS) is preempted by a crystallographic transition (low pressure rhombohedral to high pressure phase).[29] The average Sn-I bond length is known to be longer in semiconducting or insulating compounds than in metallic ones.[30] After the transition to a $Im\overline{3}$ structure, the symmetrically allowed tilting and increased distortion of the SnI_6 octahedra increases the Sn-I bond length that may result in restricting the large dispersion of the Sn $5s$ band along the ⟨111⟩ of the cubic Brillouin zone, thereby reducing the metallic character. In our system, a transition from itinerant to localized electronic state can be rationalized on the basis of the observed decrease in the B-O compressibility above 0.8 GPa. Electrical conductivity measurements under hydrostatic pressure are needed to confirm the proposed electronic transitions.

The mechanism of pressure-induced tilting and distortion of the SnI_6 octahedra can also be inferred from the observed anisotropic strain. A series of Williamson-Hall plot[31] analyses of the diffraction peaks from the $M\mathrm{SnI}_3$ data show a different pressure dependence of the lattice strain along the various crystallographic directions (Fig. 4). In particular, the strain along ⟨100⟩ appears only after the supercell transition,

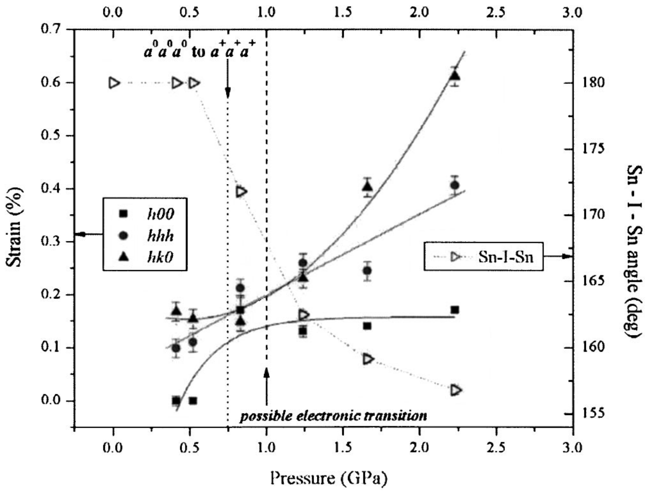

FIG. 4. Pressure dependence of lattice strain and Sn-I-Sn angle of $M\mathrm{SnI}_3$. Each data point was calculated using two to three reflections.

whereas significant amounts of strain already exist in the aristotype along the other directions. Throughout the supercell region, these strains increase further continuously while the one along $\langle 100 \rangle$ is constant. This anomalous behavior is correlated with the evolution of the framework distortions and bond compressibilities: as the symmetrically allowed tilting of the SnI_6 octahedra increases in the cubic supercell region (deviation of Sn-I-Sn connector away from $\langle 100 \rangle$), lattice strain along $\langle 100 \rangle$ is stabilized and those along non-$\langle 100 \rangle$ directions increase. The reduced compressibility of the Sn-I bond in the supercell region also gives rise to stabilizing strain along $\langle 100 \rangle$, while the accompanying electronic transition in the Sn 5s band leads to a continuing increase in stain, particularly along the $\langle 111 \rangle$ direction.

In summary, we have shown that the 3D hybrid perovskites in the tin(II)-iodine system are among the most compressible perovskites known. Unlike temperature-induced structural changes, we found no evidence of pressure-induced increased ordering of the dynamically disordered organic cations. The effect of the A-site organic cation on the overall structural change seems to be negligible at low pressures hence a ReO_3-type phase transition from a $Pm\bar{3}m$ to a $Im\bar{3}$ structure is observed. With increasing pressure, the templating effect of the organic cation becomes more important and eventually leads to the structural memory effect as observed in the reversible amorphization. The minute increase in the Sn-I bond distance and subsequent decrease in the bond compressibility observed within the $Im\bar{3}$ supercell region indicates a possible electronic localization.

ACKNOWLEDGMENTS

This work was supported by an LDRD from BNL (Pressure in Nanopores). The authors thank J. Hu and the Geophysical Laboratory for the access to their ruby laser system at beamline X17C and Patrick Woodward and Joseph Hriljac for useful discussions. Research carried out in part at the NSLS at BNL was supported by the U.S. DOE (Grant No. DE-Ac02-98CH10886 for beamline X7A).

---

[1] D. B. Mitzi, in *Progress in Inorganic Chemistry*, edited by K. D. Karlin (John Wiley & Sons, New York, 1999), Vol. 48, p. 1.

[2] D. B. Mitzi, J. Chem. Soc. Dalton Trans. **2001**, 1.

[3] A. Poglitsch and D. Weber, J. Chem. Phys. **87**, 6373 (1987).

[4] Y. Furukawa and D. Nakamura, Z. Naturforsch., A: Phys. Sci. **44**, 1122 (1989).

[5] O. Knop *et al.*, Can. J. Chem. **68**, 412 (1989).

[6] Q. Xu *et al.*, Z. Naturforsch., A: Phys. Sci. **46**, 240 (1991).

[7] N. Onoda-Yamamuro *et al.*, J. Phys. Chem. Solids **53**, 227 (1992).

[8] D. B. Mitzi *et al.*, J. Solid State Chem. **114**, 159 (1995).

[9] D. B. Mitzi and K. Liang, J. Solid State Chem. **134**, 376 (1997).

[10] K. Yamada *et al.*, Bull. Chem. Soc. Jpn. **61**, 4265 (1988).

[11] T. Vogt *et al.*, Phys. Rev. B **67**, 140401(R) (2003).

[12] D. L. Decker, S. Petersen, and D. Debray, Phys. Rev. B **19**, 3552 (1979).

[13] R. J. Angel, U. Bismayer, and W. G. Marshall, J. Phys.: Condens. Matter **13**, 5353 (2001).

[14] M. D. Welch and W. G. Marshall, Am. Mineral. **86**, 1380 (2001).

[15] H. M. Rietveld, J. Appl. Crystallogr. **2**, 65 (1969).

[16] A. Le Bail, H. Duroy, and J. L. Fourquet, Mater. Res. Bull. **23**, 447 (1988).

[17] F. Birch, Phys. Rev. **71**, 809 (1947).

[18] D. L. Decker, J. Appl. Phys. **42**, 3239 (1971).

[19] J. S. Tse *et al.*, Nature (London) **369**, 724 (1994).

[20] M. D. Rutter *et al.*, J. Phys. Chem. Solids **62**, 599 (2001).

[21] Y. Lee *et al.*, J. Am. Chem. Soc. **124**, 5466 (2002).

[22] K. S. Aleksandrov, Ferroelectrics **14**, 801 (1976).

[23] C. J. Howard and H. T. Stokes, Acta Crystallogr., Sect. B: Struct. Sci. **54**, 782 (1998).

[24] E. Suzuki *et al.*, J. Phys.: Condens. Matter **14**, 10 589 (2002).

[25] M. O'Keeffe, B. G. Hyde, and J. O. Bovin, Phys. Chem. Miner. **4**, 299 (1979).

[26] R. J. Angel, in *Reviews in Mineralogy and Geochemistry: High-Temperature and High-Pressure Crystal Chemistry*, edited by R. M. Hazen and R. T. Downs (The Mineralogical Society of America, Washington, D.C., 2000), Vol. 41, p. 35.

[27] A. M. Glazer, Acta Crystallogr., Sect. B: Struct. Crystallogr. Cryst. Chem. **28**, 3384 (1972).

[28] P. M. Woodward, Acta Crystallogr., Sect. B: Struct. Sci. **53**, 32 (1997).

[29] J. Badro *et al.*, Phys. Rev. Lett. **89**, 205504 (2002).

[30] D. B. Mitzi, Chem. Mater. **8**, 791 (1996).

[31] G. K. Williamson and W. H. Hall, Acta Metall. **1**, 22 (1953).

[32] See EPAPS Document No. E-PRBMDO-68-R03326 for supplemental figures. A direct link to this document may be found in the online article's HTML refereence section. The document may also be reached via the EPAPS homepage (http://www.aip.org/pubservs/epsps.html) or from *ftp.aip.org* in the directory /epaps/. See the EPAPS homepage for more information.